

# Graphite thin film characterization using a simplified resonant near field scanning microwave microscope

G. López-Maldonado, N. Qureshi\*, and O. V. Kolokoltsev  
*Centro de Ciencias Aplicadas y Desarrollo Tecnológico (CCADET),*  
\*e-mail: naser.qureshi@ccadet.unam.mx

H. Vargas-Hernández and C. L. Ordóñez-Romero  
*Instituto de Física, Universidad Nacional Autónoma de México,*  
*Cd. Universitaria, México D.F., México.*

Received 19 February 2013; accepted 30 September 2013

We describe a highly simplified design for a coaxial resonant near field scanning microwave microscope operating at 7.4 GHz configured to measure surface resistance and obtain topographic images with micrometer resolution. This design for a resonant probe tip combined with a highly stable mechanical system developed to rapidly tune the resonant frequency enables a simplified and effective approach to implementing near field microwave microscopy. We present images and measurements performed on a non-uniform granular graphite film sample and the surface resistance results agree with data in the literature.

*Keywords:* Near field scanning microwave microscopy; surface resistance; topographic images; resonant probe; resonant frequency.

Presentamos una descripción del diseño de un microscopio de microondas altamente simplificado de exploración por barrido con resonador coaxial que opera en el campo cercano a 7.4 GHz configurado para la medición de la resistencia superficial y la obtención de imágenes topográficas con resolución micrométrica. El diseño de una sonda altamente estable permite la sintonización rápida de la frecuencia de resonancia mediante un sistema mecánico, y esto hace posible una implementación eficiente de la microscopía de microondas de campo cercano. Las imágenes y mediciones presentadas corresponden a una película de grafito granular no uniforme cuya resistencia superficial medida concuerda con los datos reportados en la literatura.

*Descriptores:* Microscopía de microondas de campo cercano; resistencia superficial; imágenes topográficas; sonda resonante; frecuencia resonante.

PACS: 78.70.Gq.

## 1. Introduction

Near field microwave microscopy (NFMM) has attracted attention in recent years due to its sub-micrometer resolution and its utility in characterizing electrical properties of a variety of materials relevant to microelectronics [1-4] and the biological sciences [5]. It has yet to gain widespread acceptance as a routine characterization technique partly due to the complexity involved in interpreting images [6,7]. One approach has been to implement NFMM systems based on planar microwave probes integrated with commercial atomic force microscopes [8,9], which allows one to make use of existing scanning systems. Although this approach has led to the highest resolutions reported to date [10] and is the basis of a commercial system (Agilent), it is especially costly. A more common approach has been to implement systems based on coaxial resonant probes [12] which are much simpler from an electromagnetic point of view and are easier to fabricate.

The design of microwave scanning near field probes fall into two categories: broadband and resonant [11]. The vast majority of recent works have focused on resonant systems which provide a much higher energy density at the probe tip and allow for sensitive cavity perturbation measurements sensitive to both the real and imaginary parts of the sample impedance [13-15]. The response of a resonant system to the interaction with a sample has been used to obtain super-

ficial topography images [16] and to measure electrical [17] and magnetic [18,19] properties of planar samples, typically capacitance associated with changes in frequency and resistance associated with changes in quality factor [20,21]. Spatial resolution is determined by tip sharpness, which also influences the sensitivity with which cavity perturbation parameters need to be measured.

This work responds to the need for an accessible NFMM system and a simple and robust protocol for interpreting images. We describe a system based on the well studied coaxial geometry [11], with a new and particularly simple implementation that allows for an easily tunable probe and easily interchangeable probe tips. Additionally, a method is described for the fabrication of micrometer resolution probes using a simple, repeatable mechanical technique. Here we choose a representative sample with variations both in sheet resistance and in topography: a thin film of graphite on a glass substrate with a thickness much less than the skin depth at 7.4 GHz. We present spatially resolved measurements of surface resistance and provide an interpretation of electromagnetic properties of the sample through a simple mathematical model derived here.

## 2. Experimental procedures

A block diagram of our system is shown in (Fig. 1). Microwave power from a network analyzer (Agilent E5071C)

was supplied to a resonant near field probe through a directional coupler, whose output reflection port was connected to a microwave amplifier. This output signal was sent to a detector diode, whose d.c. signal, proportional to the microwave power, was amplified and filtered through a low noise preamplifier (SRS560). A three-axis motorized translation stage system, with a resolution of 10 nm per step [22] allows for both two dimensional scanning over the sample and control over the probe-sample distance. The network analyzer's detection system was used to measure the probe's reflection coefficient ( $\Gamma$ ) in the absence of a directional coupler and the frequency was then fixed to a point on the resonant curve where the reflected power was about half its maximum value. As in previous works [2,5], when the reflected signal is then sent to the diode detector, one can assume that small changes in resonant frequency give rise to changes in the measured microwave power in a quasi-linear fashion. When the tip is brought close to a sample, its coupling to the sample perturbs the cavity and results in a change in resonant frequency. The reflected power is thus used, once digitized and with appropriate software, to create an image representing frequency shift at each point over which the probe is mechanically scanned. In this way, it is not necessary to measure the entire cavity resonant spectrum at every point in an image, which is an important simplification.

Our near field probe tip was constructed from a short segment of a commercial cylindrical coaxial microwave transmission line whose external conductor diameter was 1.22 mm and internal conductor diameter was 0.28 mm. Its cross section was much smaller than the wavelength used, which allows only TEM wave propagation. Its length of the coaxial segment was close to the wavelength of the incident radiation. Its input port was formed by a flat and polished central conductor to permit capacitive coupling to the microwave feeder line, while the near field probe section was left open with the protruding central conductor ending in a sharp tip (Fig. 2). This probe tip was manufactured using a purely mechanical

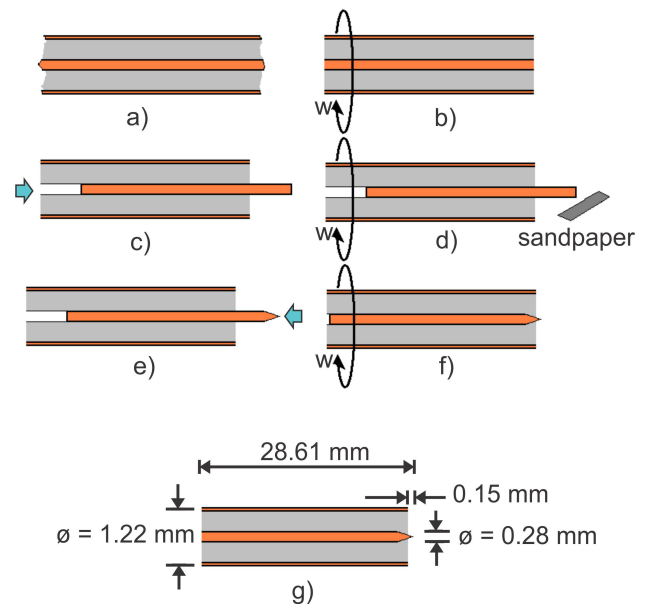


FIGURE 2. Schematic of the process used in tip fabrication.

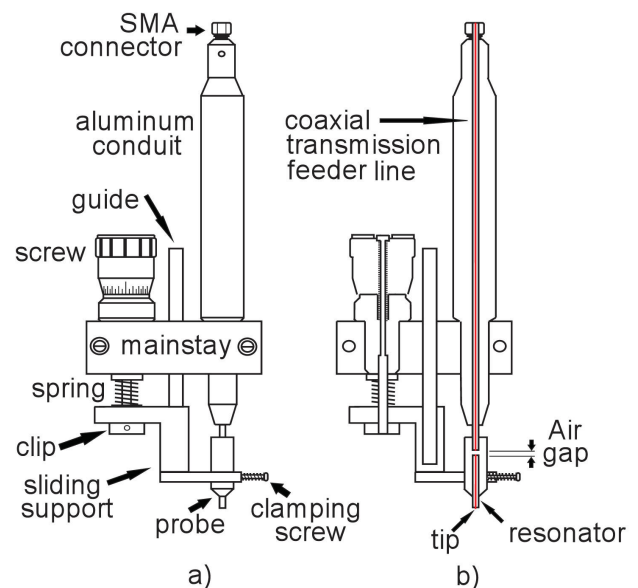


FIGURE 3. Details of the tuning system showing a) the mechanical adjustment and b) the coaxial resonator.

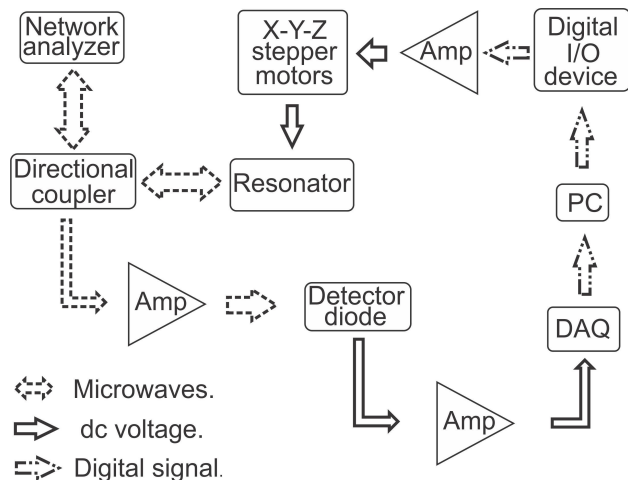


FIGURE 1. Schematic of the experimental setup showing the electronic and microwave components.

procedure: a section of transmission line (Fig. 2a) was mechanically polished on both sides (Fig. 2b), a portion of the central conductor displaced (Fig. 2c), and the protruding section was mechanically turned in a precision lathe to form a sharp tip (Fig. 2d). The central conductor was then brought close to its initial position with the tip protruding less than 150 microns (Fig. 2e) from the outer conductor, the opposite end was polished again (Fig. 2f) and the probe tip was assembled with the tuning system. Its dimensions are also shown (Fig. 2g). An important feature of this design is the fact that the central conductor is easy to extract, which makes it easy to replace tips and to sharpen and reuse damaged tips.

To allow for fast tuning of the probe tip’s central frequency, while maintaining frequency stability, we developed a mechanical tuning system shown in (Fig. 3). By turning the micrometer screw shown in (Fig. 3b), the coupling of the input section of the resonator to the microwave feeder is adjusted by varying the air gap between the two coaxial lines. This not only varies the depth of the resonance peak in the reflected signal at resonance, but also allows us to tune the central frequency and, to some extent, the loss suffered by the cavity to the feeder line. This provides an important operational advantage: not only do we have fine control over the resonant frequency, but also over the width of the resonant peak, as a result of this precisely controlled coupling between the resonator and the feeder line. The latter makes it possible to optimize the cavity parameters so that the frequency displacement caused by a given sample is always less than the width of the resonant peak, and the quasi-linear approximation described above is always valid. This detail is important: the quasi-linearity allow us to make quantitative estimations of the sample properties without having to measure the full reflection spectrum at each point in an image, as shown in the next section. Additionally, the tuning of the cavity of course affects the sensitivity and signal to noise ratio, by varying the extent of the change in measured reflected power caused by a given sample.

### 3. Results

In order to extract meaningful information from the instrument, the microwave properties of the resonator were first characterized. To this end, we rely on a simple model of the resonator and tip. As shown in (Fig. 4a), we assume there is a well defined coupling between the feeder line and resonator

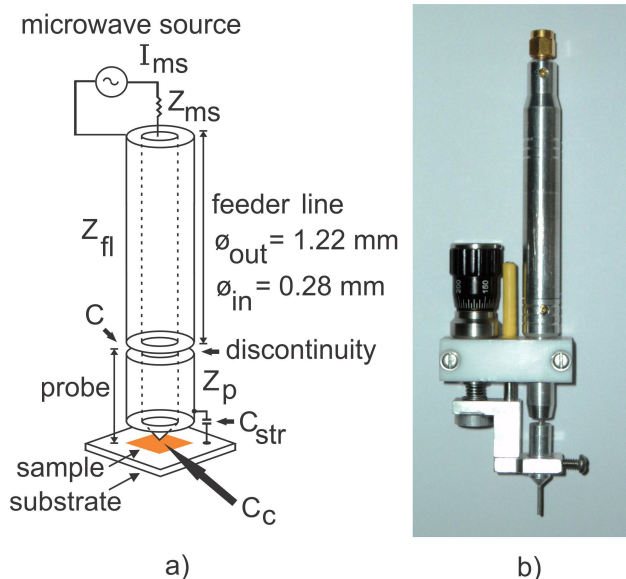


FIGURE 4. a) A distributed parameter model used to describe the microwave behavior of the system, b) a photograph of the tuner system.

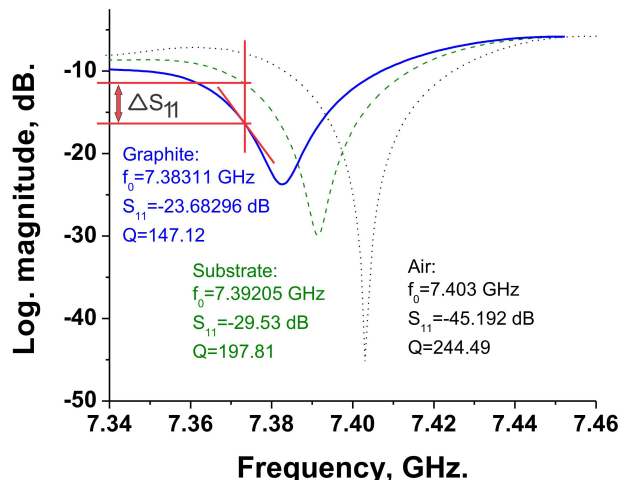


FIGURE 5. Experimentally observed resonant behavior of the system for the bare resonator (dotted line), the tip in close proximity to a glass substrate (dashes line) and the tip in close proximity to a graphite sample (solid line). Also shown is the change in cavity reflection measured at a fixed frequency when the tip moved from the substrate to the graphite.

onator with capacitance  $C$ , there is a capacitance  $C_c$  between the tip and the sample and a stray capacitance  $C_{str}$  between the outer conductor and the sample. For clarity, an image of the tuner system is shown in (Fig. 4b).

The cavity absorption curve was obtained by measuring directly the complex reflection coefficient  $\Gamma$  versus frequency (also known as  $S_{11}$ ). The discontinuity between the feeder line and the probe was maintained at the condition of critical resonant coupling so that impedances between the microwave source  $Z_{ms}$ , the feeder line  $Z_{ft}$  and the probe tip  $Z_p$  were matched with effective impedance  $Z_0 = 50$  Ohm

First, the resonant frequency  $f_r$ , defined as the frequency of minimum reflection, was measured for the resonator alone. This yielded a frequency of 7.403 GHz with a small minimum reflected power of -45.192 dB. The procedure was repeated with the probe tip in close proximity to a glass substrate (with a separation of a few microns), and then again with the probe tip close to a thin structure of patterned graphite on a glass substrate. The results are shown in (Fig. 5): In the first case, with the probe tip in air, we observe the highest quality factor  $Q$  and frequency. With the tip close to glass, we observe a decrease in both resonant frequency and  $Q$ , and a further decrease when close to graphite. We also find that there is a convenient frequency point in the spectrum where the frequency shift gives rise to an approximately linear change in measured reflected power. The validity of this will be tested at below by comparing the final measurement with known sample parameters.

The nature of the interaction between the tip and sample was characterized further by investigating the complex impedance of the reflected signal. The results are summarized in the Smith charts shown in (Fig. 6): we observe that

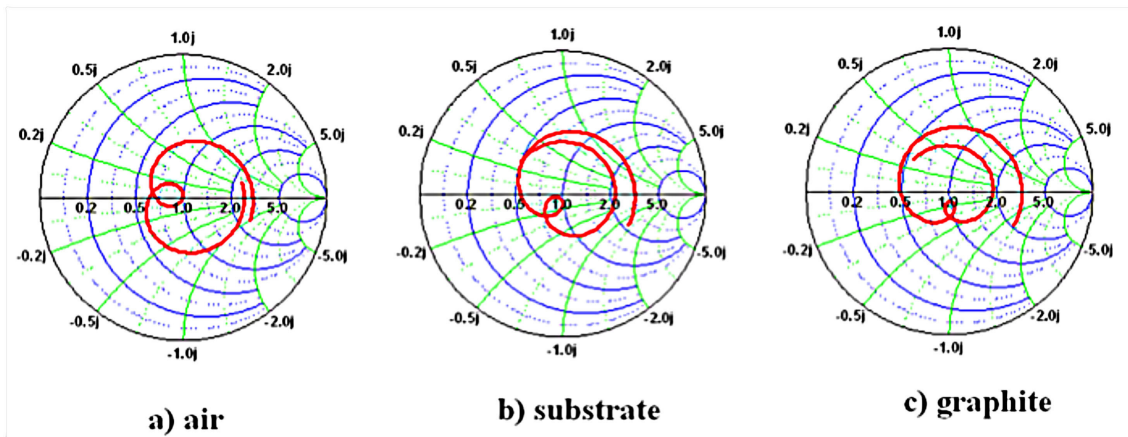


FIGURE 6. Smith charts showing the complex reflectance of the resonator.

TABLE I. Cavity perturbation parameters for a tip close to the sample.

	$f_{r_{fit}}$ (GHz)	$Q$	$\eta_Q$ %
Air	7.40329	244.49	–
Subst	7.39042	197.81	19.10
Graph	7.3795	147.12	39.82

the coupling changes from inductive in air to capacitive in presence of the graphite sample. It is clear that the effect of both the substrate and the graphite film is to change both the frequency and phase of the signal reflected from the resonator. This gives us the option of using both phase and frequency to deduce material properties of the sample. In this work we choose frequency, since it implies a simpler measurement and therefore a simpler instrument.

It is clear from these results that the resonator provides sensitivity to changes in quality factor and resonant frequency that can be measured using the method described in the previous section. These properties are summarized in Table I: the

resonant frequency shifts as determined through a Lorentzian fit and the quality factor. The probe tip efficiency, defined as  $\eta_Q = 1 - Q_m/Q_{air}$  [25], is also shown and this provides a measure of the degree to which the cavity is being perturbed. In this case, the perturbation is substantial.

The extent to which the sample perturbs the resonant cavity depends on the tip-sample distance. This was verified by repeatable measurements performed at different heights at a fixed point on the surface of graphite as shown in (Fig. 7). In Table II we condense the relevant experimental information. In particular, the maximum variation of  $Q$  when the probe tip interacts with graphite is from 0 to  $0.5 \mu\text{m}$  and here the sample is effectively part of the resonant circuit.

The coupling between the probe-tip and the sample is through capacitance  $C_c$  (Fig. 4), which depends strongly with the distance  $d$ . An increase in capacitance (and loss) leads to greater absorption and a reduction in resonant frequency. In Table II,  $\Delta f$  variation is greatest at the minimum distance (0.25 microns), which implies a maximum change in capacitance, and in this condition topographic images were obtained from shifts in capacitance during tip scanning. It

TABLE II. Cavity perturbation parameters as a function of tip-sample distance with a graphite sample.

Height ( $\mu\text{m}$ )	$f_{r_{fit}}$ GHz	$\Gamma$ dB (Experimental)	$Q$	$\Delta f_{r_{fit}}$ MHz (In relation to $f_{r_{fit}}$ in air)
0.0	7.37487	-21.535	130.73	28.42
0.25	7.37950	-23.680	147.12	23.79
0.5	7.38553	-24.723	170.10	17.76
1.0	7.38873	-26.244	185.09	14.56
2.0	7.39107	-27.445	196.93	12.22
4.0	7.39370	-29.115	209.04	9.59
5.0	7.39446	-29.432	212.12	8.83
10.0	7.39703	-30.417	223.13	6.26
$\infty$ final measue.	7.40329	-45.192	244.49	0.00

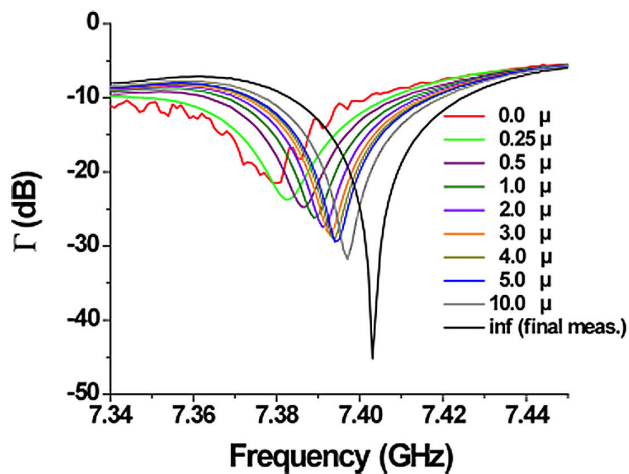


FIGURE 7. Behavior of the cavity reflectance when the probe tip is placed above a graphite surface and the vertical distance between tip and sample is varied.

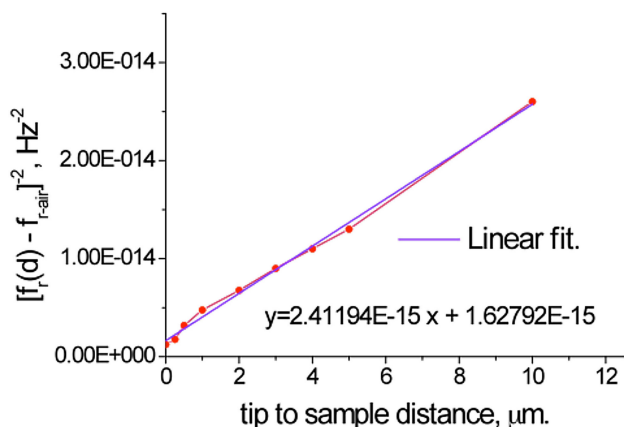


FIGURE 8. Plot of sample separation vs.  $[f_r(d) - f_{r-air}]^{-2}$  with a graphite sample.

is worth noting that the tip-sample separation has a much stronger effect on the response than any reasonable change in graphite impedance, and we use this fact to distinguish between the effects. For this reason, we can safely say that scanning with over an amorphous surface will produce predominantly topographic images.

It is instructive to consider the tip-sample interaction from a dimensional point of view. The frequency of a simple resonator is proportional to  $1/(LC)^{1/2}$ , and the capacitance of the tip-sample region is proportional to  $1/d$  (assuming the tip and sample can be modeled effectively as parallel plates). Since the capacitance of this region adds linearly to the capacitance of the resonator (two capacitors in series), the frequency shift is proportional to  $[f_r(d) - f_{r-air}]^{-2}$  where  $f_r(d)$  is the resonant frequency at any given value of  $d$  and  $f_{r-air}$  is the resonant frequency of the resonator alone. Inserting values from Table II, and fitting, we obtain the curve in Fig. 8, which is consistent with this simple physical interpretation. The close agreement confirms that the tip-sample interaction can be seen as a simple capacitive one, and can be described in a lumped circuit model, as we do in the next section.

By scanning the tip over the graphite structure on a glass substrate in two dimensions and recording the change in reflected microwave power at a fixed frequency, images were obtained. The tip-sample separation was fixed at  $0.25 \mu\text{m}$  above the graphite structure. A representative image is in (Fig. 9a). Scanning above of the graphite we can distinguish different intensities of blue corresponding to surface variations detected as changes in  $\Gamma$ , dark corresponds to more reflected power. (Fig. 9b) shows a three-dimensional surface representation of the image obtained. This shows clearly the topographic distribution of thin areas of graphite on the glass substrate. In the next section, we extract the value of surface resistance as a function of these data.

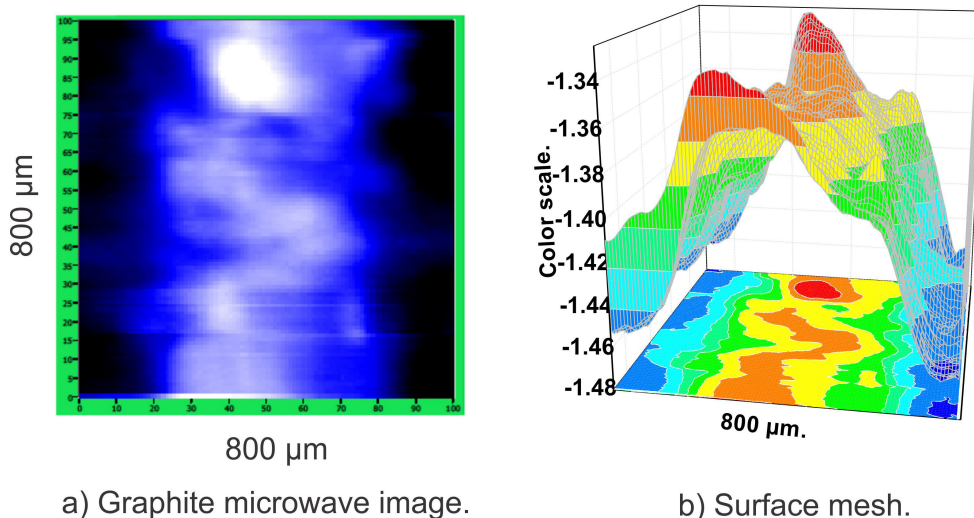


FIGURE 9. A representative image of a graphite sample on glass substrate. In contour plot (a), white and blue correspond to graphite of varying density and white corresponds to the glass substrate. Surface plot (b) indicates the relative magnitude of the change in reflection coefficient on a linear scale with arbitrary units.

## 4. Discussion

A simple model derived from standard transmission line theory [23] was used to determine the surface resistivity of the graphite  $\rho_{g-sr}$  at a local point employing these measurements and estimations. Initially we relate the experimental measured reflection coefficient  $\Gamma$  obtained with the network analyzer to the probe tip characteristics then we relate this result to the impedance of the sample.

With the system in operation the probe tip simultaneously interacts with the feeder line and with sample. First we consider the interaction between the feeder line and the resonator. The resonance condition is [23]

$$\exp(-i2hL)\Gamma\Gamma_0 = \exp(-i2\pi n), \quad (1)$$

in which  $\Gamma$  is the complex reflection coefficient from the probe tip opposite end to the feeder line,  $h = h' - h'' = \omega(\varepsilon_0\varepsilon_{eff}\mu_0)^{1/2} - ih''$  with  $h' \gg h''$  is the transmission line complex propagation constant [23],  $\omega = 2\pi f_r$ ,  $\varepsilon_0 = 8.854 \times 10^{-12}$  F/m and  $\mu_0 = 4\pi \times 10^{-7}$  H/m are the permittivity and permeability of the vacuum respectively,  $\varepsilon_{eff} = 3.147$  is the effective dielectric constant of the transmission line calculated using standard methods,  $L = 0.02861$  m is the length of the resonator and  $n$  is the mode number.

Next, the complex reflection coefficient between the probe tip and the sample is given by

$$\Gamma_0 = \frac{Z_s - Z_p}{Z_s + Z_0}, \quad (2)$$

where  $Z_s$  is the effective impedance of the sample and  $Z_0$  is the effective impedance of the probe tip. In the intermediate regime [3,13]  $\rho_{g-sr}/Z_{subst} \ll t_g \ll \delta_g$  is satisfied, which gives rise to

$$Z_s = \rho_{g-sr}/t_g. \quad (3)$$

Here,  $Z_{subst}$  is the effective complex impedance of the substrate, and  $t_g$  and  $\delta_g$  are the thickness and the penetration depth of the graphite film respectively.

In order to obtain  $\Gamma_0$  in terms of  $\rho_{g-sr}$  Eq. (4) is substituted into Eq. (2) which results in

$$\Gamma_0 = \frac{\rho_{g-sr} - Z_0 t_g}{\rho_{g-sr} + Z_0 t_g}. \quad (4)$$

It is important to note that the magnitude of  $\Gamma_0$  will depend strongly on the distance between the tip and the sample, bringing the tip closer to the sample will increase the sensitivity. Here, we can use the measured values of  $Q$  from Table II.

Now substitution of Eq. (4) into Eq. (1) relates the probe tip characteristics with the graphite superficial resistivity, solving for  $\rho_{g-sr}$  we obtain

$$\rho_{g-sr} = \frac{Z_0 t_g [\exp(-i2\pi n) + \exp(-i2\pi L)\Gamma]}{\exp(-i2hL)\Gamma - \exp(-i2\pi n)}. \quad (5)$$

Equation (5) depends now on the properties of the resonator, the thickness of graphite, the suitable impedance coupling, and depends on  $\Gamma$ . This allows us to extract the surface resistivity directly from the microwave measurements.

With this simple model, we can estimate the surface resistivity of the graphite sample from the experimental results when the height between the probe tip and the graphite is  $0.25 \mu\text{m}$ . Using Eq. (1), and substituting  $\varepsilon_{eff} = 3.147$  and  $h = 274.5 - .02741i$  from the previous section, we find that the experimental complex reflection coefficient from the resonator opposite end to the feeder is  $\Gamma = 50.00 - 6.414i$ . Note that the cross sectional geometry is chosen to be much smaller than the wavelength, therefore the TEM mode is the only possibility and we use mode number  $n = 1$ . This value can then be substituted into Eq. (5), and using a measured average graphite thickness of  $0.270 \mu\text{m}$  to calculate the surface resistance. This yields to  $\rho_{g-sr} = 14.1621 \times 10^{-6} \Omega/\text{m}$  which is in good agreement with reported data of  $14.286 \times 10^{-6} \Omega/\text{m}$  [24].

Note that this result corresponds to one point on the sample with known graphite thickness. Clearly, this procedure can be repeated in an automated manner to quantify the surface resistance at each point on an image such as that in (Fig. 8). Alternatively, taking advantage of the good quantitative agreement between our calculation and the correct value of surface resistance, this procedure can also be applied in reverse: from Eq. (5) we can estimate the thickness of the graphite film if we know the value of the surface resistance.

## 5. Conclusions

We have demonstrated the functionality of a highly simplified microwave microscope, and have shown that a simple theoretical treatment provides an effective way to determine the correct surface resistance of a sample with complex impedance, with spatial resolution at the micrometer scale. The main contribution of this work is the combination of a simple and reliable method for fabrication of a resonant probe-tip, a simplified method for implementing a rapid tuning mechanism and a theoretical treatment that agrees closely with known values of surface impedance. This represents a step towards the practical application of microwave microscopy in routine measurements.

## Acknowledgement

This work was supported by PAPIIT UNAM, project IN104513. The authors are grateful to Agilent, Mexico, for their generous assistance with microwave measurements.

1. T. Wei, X. -D. Xiang, W. G. Wallace-Freedman and P. G. Schultz, *Appl. Phys. Lett.* **68** (1996) 3506.
2. M. Tabib-Azar and D. Akinwande, *Rev. Sci. Instrum.* **71** (2000) 1460.
3. M. Park, H. Yoo, H. Yoo, S. Na, S. Kim, K. Lee, B. Friedman, E. Lim and M. Iwamoto, *Thin Solid Films* **499** (2006) 318.
4. C. Gao and X. -D. Xiang, *Rev. Sci. Instrum.* **69** (1998) 3846.
5. M. Tabib-Azar, P. S. Pathak, G. Ponchak and S. LeClair, *Rev. Sci. Instrum.* **70** (1999) 2783.
6. R. A. Kleismit, M. K. Kazimierczuk and G. Kozlowski, *IEEE Trans. on Microwave Theory and Tech.* **54** (2006) 639.
7. A. Imtiaz, S. M. Anlage, J. D. Barry and J. Melngailis, *Appl. Phys. Lett.* **90** (2007) 143106-1.
8. M. Tabib-Azar and Y. Wang, *IEEE Trans. on Microwave Theory and Tech.* **52** (2004) 971.
9. D. W. van der Weide, *Appl. Phys. Lett.* **70** (1997) 677.
10. M. Tabib-Azar, D. -P. Su, A. Pohar, S. R. LeClair and G. Ponchak, *Rev. Sci. Instrum.* **70** (1999) 1725.
11. B. T. Rosner and D. W. van der Weide, *Rev. Sci. Instrum.* **73** (2002) 2505.
12. C. P. Vlahacos, R. C. Black, S. M. Anlage, A. Amar and F. C. Wellstood, *Appl. Phys. Lett.* **69** (1996) 3272.
13. M. Abu-Teir, M. Golosovsky, and D. Davidov, *Rev. Sci. Instrum.* **72** (2001) 2073.
14. J. Kim, K. Lee, B. Friedman and D. Cha, *Appl. Phys. Lett.* **83** (2003) 1032.
15. J. Kim, M. S. Kim, K. Lee, J. Lee, D. Cha and B. Friedman, *Meas. Sci. Technol.* **14** (2003) 7.
16. C. P. Vlahacos, D. E. Steinhauer, S. K. Dutta, B. J. Feenstra, S. M. Anlage and F. C. Wellstood, *Appl. Phys. Lett.* **72** (1998) 1778.
17. D. E. Steinhauer, C. P. Vlahacos, S. K. Dutta, B. J. Feenstra, F. C. Wellstood and S. M. Anlage, *Appl. Phys. Lett.* **72** (1998) 861.
18. K. Lee, H. Melikyan, A. Babajanyan, T. Sargsyan, J. Kim, S. Kim and Barry Friedman, *Ultra-microscopy* **109** (2009) 889.
19. S-C. Lee, C. P. Vlahacos, B. J. Feenstra, A. Schwartz, D. E. Steinhauer, F. C. Wellstood and S. M. Anlage, *Appl. Phys. Lett.* **77** (2000) 4404.
20. A. Tselev, S. M. Anlage, Z. Ma and J. Melngailis, *Rev. Sci. Instrum.* **78** (2007) 044701-1.
21. P. J. Petersan and S. M. Anlage, *J. Appl. Phys.* **84** (1998) 3392.
22. N. Qureshi, O. V. Kolokoltsev, R. Ortega-Martinez, C. L. Ordóñez-Romero and J. M. Saniger, *J. Nanosci. Nanotechnol.* **8** (2008) 6466.
23. S. M. Anlage, V. V. Talanov and A. R. Schwartz, *Principles of Near-Field Microwave Microscopy, in Scanning Probe Microscopy: Electrical and Electromechanical Phenomena at the Nanoscale*, vol. 1, (Springer-Verlag, New York, 2007), pp. 215-253.
24. D. M. Pozar, *Microwave Engineering*, 3rd ed. (John Wiley&Sons, USA, 2005). pp 687.
25. M. Mehdizadeh, *Microwave/RF Applicators and Probes*, (Elsevier, Great Britain, 2010). pp 24 56.